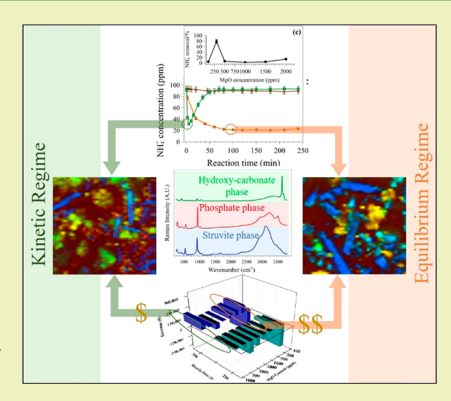


Transient Struvite Formation during Stoichiometric (1:1) NH₄⁺ and PO₄3- Adsorption/Reaction on Magnesium Oxide (MgO) Particles

Daniyal Kiani, Yiying Sheng, Baoying Lu, Dovydas Barauskas, Kenneth Honer, Zhe Jiang, and Jonas Baltrusaitis*, Too

ABSTRACT: Nitrogen (N) and phosphorus (P) nutrient recovery in a solid form from wastewater streams is of utmost importance while managing their global cycles. Here, we show that water insoluble MgO precursor can be utilized to synthesize MgNH₄PO₄·6H₂O (struvite). Hence, water-soluble magnesium precursors, such as MgCl₂, that require expensive synthesis routes can be substituted with more sustainable, naturally occurring but less soluble magnesium precursors, such as MgO. Time-resolved analysis of solid and liquid products showed two MgO concentration regimes during struvite formation, e.g. a kinetically controlled one at [Mg:NH₄⁺:PO₄³⁻] ratio of 4.80:1:1 and an equilibrium limited one at [Mg²⁺]: $[NH_4^+]$: $[PO_4^{3-}] = 1.44:1:1$. In both cases, >70% of NH_4^+ and PO_4^{3-} species were removed from solution with the pseudo-second-order dependence of the reaction rate on the starting MgO concentration. The dual adsorption/reaction behavior of both ions needed in equimolar amounts to form struvite resulted in heterogeneous product distribution with magnesium phosphate as the dominant component at



equilibrium. Spatially resolved Raman and pXRD analyses showed that crystalline struvite (MgNH₄PO₄·6H₂O), magnesium phosphate (Mg₃PO₄·22H₂O) and complex amorphous species are present. The Raman spectral footprint of the intermediate component was assigned to dypingite, Mg₂(CO₃)₄(OH)₂·4H₂O. This suggests that parallel hydration reaction takes place, under ambient conditions, to form magnesium hydroxycarbonates when excess MgO is available. In turn, this implies that various carbonates of magnesium can potentially be utilized with improved conversion during struvite precipitation from aqueous N and P precursor solutions. Lastly, sustainability and economic analysis of struvite synthesis from MgO clearly showed that employing MgO instead of MgCl₂ can significantly decrease overall energy requirements, and the resulting carbon footprint by a factor of ~ 3 .

KEYWORDS: Struvite, Nitrogen, Phosphorus, Raman, XRD, Magnesium oxide

INTRODUCTION

The world population growth is accompanied by an unprecedented demand for food, which results in increased natural resource use. One such constrained resource is the agricultural land available to produce food with farmers relying on fertilizers to sustain and increase food production from effectively fixed land size.² In particular, increasing crop and livestock production are the largest causes of the global nitrogen (N) and phosphorus (P) cycle change due to the large surplus of both nutrients to the environment via mineral fertilizer influx.³ Typically, surplus N is lost to the environment in the form of greenhouse gas emissions, such as ammonia (NH_3) , nitrous oxide (N_2O) , and nitric oxide (NO).^{4,5} Surplus P, which is much less soluble and reactive, is lost via runoff and enters the watershed to be transported into freshwater and coastal marine reservoirs, causing hazardous eutrophication. Alternately, it can also accumulate as residual soil P.6,7 This way, half a billion tons of P has been deposited in the hydrosphere, mainly due to the overuse of P fertilizers.^{8,9}

These losses are compounded by the large amounts of energy necessary for N and P fertilizer production. N fertilizers are particularly energy intensive to produce via NH3 synthesis which consumes about 1-2% of the total global energy and 3-5% of total natural gas. ^{10,11} P fertilizers, on the other hand, are derived via mining phosphate rock. According to some reports, the world will run out of phosphate rock in the next 50-100 years due to heavy mining. 7,8 P has no substitute, since it cannot be created or destroyed and is not sustainably utilized.^{7,12} As a result, a shift from mined sources of P toward fertilizers produced from sources recycled from within the human food chain needs to take place. 8,13 Waste sources, such as animal manure, collected in lagoons, deep pits, or other collection vessels, could conceivably be processed to recycle P. 14 Furthermore, agricultural and food industry related

Received: October 15, 2018 Revised: November 20, 2018 Published: November 23, 2018

1545

[†]Department of Chemical and Biomolecular Engineering, Lehigh University, B-336 Iacocca Hall, 111 Research Drive, Bethlehem, Pennsylvania 18015, United States

^{*}Medical College, Guangxi University of Science and Technology, 1301 Medical Building, 257 Liushi Street, Liuzhou, Guangxi 545000, China

wastewater contains significant amounts of N and P in the form of $\mathrm{NH_4}^+$ and $\mathrm{PO_4}^{3-}$ ions, respectively. Typically, N/P mass ratio in such wastewater streams ranges from 3 to 11. Therefore, simultaneous removal of both $\mathrm{NH_4}^+$ and $\mathrm{PO_4}^{3-}$ from wastewater streams is needed in N and P recovery to provide a more sustainable route of fertilizer manufacturing.

Widely used, mature technologies for N and P removal from wastewater streams include biological nitrification/denitrification for N removal and insoluble metal salt precipitation for P removal. 16 Both approaches result in the removal of nutrients in a manner that leaves them unsuitable for reuse. Recovery of nutrients in a concentrated solid form, such as sparingly watersoluble (169.2 mg L⁻¹)¹⁷ crystalline struvite (MgNH₄PO₄· 6H₂O), is desirable due to the ease of handling, transportation, storage, and controlled reuse with an added benefit of the reduced pathogen risk. 18 As struvite crystals are composed of equimolar parts of magnesium, ammonium, and phosphate, this fertilizer product can serve as an effective fertilizer for food crops. 19 Struvite crystals are formed from aqueous solutions of precursors at a pH of 8.0–9.5. ^{20,21} Crystal growth conditions, including pH, ²² solid retention time, ²³ saturation level, and the use of particle-growth seed,²⁴ affect the morphology and particle size of the recovered struvite. For effective struvite crystallization, N and P containing wastewater solution must contain phosphate (PO₄³⁻), ammonium (NH₄⁺) and magnesium (Mg^{2+}) ions in close to equimolar (1:1:1) ratio^{25,26} with external Mg source added. The key to the cost-effective and sustainable struvite recovery is the nature of the Mg source. Although Mg is a common constituent of many minerals, comprising 2% of the earth's crust, most soil Mg (~98%) is incorporated in the crystal lattice structure of low solubility minerals and thus is not directly available for plant uptake.² Predominantly water-soluble Mg salts, such as MgCl₂ and MgSO₄, which comprise only a small portion of the natural magnesium containing minerals, are used for N and P recovery and account for up to 75% of the struvite production cost.²⁸ Industrially, MgCl2 is mostly prepared from ocean, seawater or lake brine via reaction with HCl²⁹ as in Dow process, followed by precipitation, purification, and other energy intensive and expensive processes.³⁰ On the other hand, low water solubility MgO (periclase) and MgCO₃ (magnesite) are present in abundant quantities naturally. The United States Geological Survey estimates worldwide resources of magnesite close to 12 billion tons.

To decrease the economic and environmental cost of industrial struvite production from wastewater, insoluble, cheap and abundant Mg sources such as MgO or MgCO3 need to be used instead of soluble but expensive MgCl2 and MgSO₄. Previously, some fundamental, proof-of-concept studies have been conducted to show the feasibility of using such insoluble Mg sources in struvite production.³²⁻ Capdevielle, Biscans and co-workers utilized MgO suspension to derive optimal operating parameters of struvite formation from synthetic swine manure. 33,35 A rapid pH decrease to 10.7 followed by a continuous increase to 11 took place which suggested hydration/dissolution of MgO to form Mg(OH)2. Measured Mg²⁺ concentration profile, however, decreased to low values and stayed constant regardless of the pH, suggesting that any dissolved Mg²⁺ is immediately consumed. An alternative mechanistic explanation was offered by Kirinovic et al.³² where amorphous intermediate material was observed within a short (1-5 min) time frame of the reaction onset implying that direct heterogeneous transformation of MgO and

 ${\rm MgCO_3}$ into struvite is possible. Other recent studies 36,37 utilized low solubility Mg sources, such as MgO, and showed varying results of ${\rm PO_4}^{3-}$ and ${\rm NH_4}^+$ removal depending on the source of the material, likely linked to the physical state, such as particle size, of the initial particles and the resulting diffusion/solubility limitations. Additional sources afforded to utilize solid metallic Mg electrode as a source of magnesium, 38,39 noting that it is difficult to cost compete with Mg salts or MgO. 39

However, in-depth analysis of kinetics and the mechanics of struvite formation from insoluble Mg precursors is needed, as differences are expected due to the presumably slow dissolution of MgO needed.^{7,32} In the present study, we report insights into struvite formation from simulated wastewater using insoluble MgO precursor, studied with ion chromatography (IC), powder X-ray diffraction (pXRD), and ex situ Raman spectroscopy (RS). We show that excess of MgO, proposed due to the slow dissolution step, ^{33,36,38,7} is not always used as a kinetic control of the product at short reaction times. Hence, the emphasis is on the physical phenomena taking place before the equilibrium of the reaction. A technoeconomic evaluation of using insoluble Mg sources versus soluble MgCl₂ for industrial scale struvite production as well as the sustainability metrics of substituting MgCl₂ with MgO are also presented.

■ EXPERIMENTAL METHODS

lon Chromatography (IC). The Metrohm Eco 925 ion chromatography system (Herisau, Switzerland) was used in all experiments. Separation columns used were Metrosep A supp 4/5 Guard column (5 × 4 mm), Metrosep A supp 5 (4 × 150 mm) for anion analysis, and Metrosep C 4 Guard column (5 × 4 mm) and Metrosep C 4 (4 × 150 mm) for cation analysis. The sample-loop volume was 10 μ L in the cation system and 20 μ L in the anion system, and eluted species were measured using a conductivity detector. Here, 1.75 nM HNO₃ and 0.7 mM DPA were used as eluent for Metrosep C 4, while 3.2 mM Na₂CO₃ and 1.0 mM NaHCO₃ were used for Metrosep A supp 5. All samples were measured at room temperature. Error bars are provided for triplicate experiments. The system was computer controlled through MagIC Net 3.2 software.

Powder X-ray Diffraction (pXRD). The crystalline nature of all reactants and products was confirmed using powder X-ray diffraction (Empyrean, PANalytical B.V.). The applied current was 40 mA, and the applied voltage was 45 kV. The X-ray mirror that was used was a graded, flat Bragg—Brentano HD mirror, and the step size that was used for the measurements was 0.0131°.

Raman Spectroscopy. Raman spectra and spectral maps were acquired using the WITec alpha300R confocal Raman microscope using 532 nm laser and 100× objective. Laser intensity at the sample was ~54 mW. True Component Analysis (TCA) was used to create the spectral intensity distribution images of different spectra components. It utilizes a linear combination of the spectral components using the basis analysis algorithm via eq 1

$$\vec{S}_i = \hat{B}\vec{H}_i + \vec{E}_i \tag{1}$$

where \vec{S}_i is spectrum i from the spectral data set, \hat{B} is the matrix of basis spectra, \vec{H}_i is mixing values of spectrum i, and \vec{E}_i is the error spectrum. The mixing values are fitted using least-squares minimization methods following eq 2:

$$(\vec{S}_i - \hat{B}\vec{H}_i)^2 = \text{minimum} \tag{2}$$

This method allowed identification of unique spectral components that comprised Raman data sets.

Reagents and Solutions. Stock solutions of ammonium (1.0 g/L), magnesium (1.0 g/L), and phosphate (1.0 g/L), were prepared from monoammonium phosphate $NH_4H_2PO_4$ (MAP, 99.9%+, Fisher

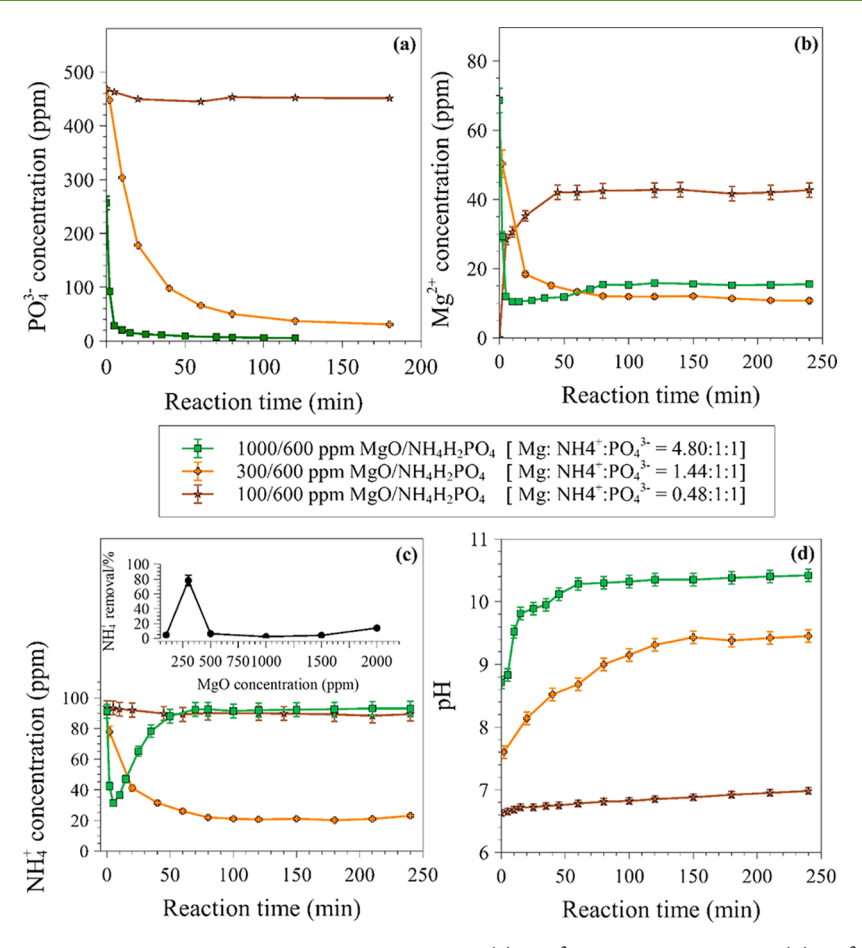


Figure 1. Ion concentration as a function of reaction time, measured using IC. (a) PO_3^{3-} anion concentration, (b) Mg^{2+} cation concentration, (c) NH_4^+ cation concentration, and (d) change in pH of solution during struvite growth, with different starting MgO concentration. Initial 600 MAP solution pH was 5.4.

Scientific) and MgCl₂ (99.9%+, Fisher Scientific). Appropriate amounts of individual salts were weighted into a volumetric flask (100 mL) and dissolved in deionized (DI) water. Working standard solutions of ammonium, magnesium, and phosphate were prepared by measuring the appropriate volume of standard solutions into a 100 mL volumetric flask which was afterward filled with DI water. Working eluent solutions were prepared by appropriate dilution of standard eluent solution with DI water. A 18.2 M Ω /cm DI water (Millipore, Bedford, MA) was used for dilution in all cases. MgO powder (99%+) was obtained from Sigma-Aldrich and used as received.

Struvite Synthesis. Struvite synthesis from simulated wastewater was performed using magnesium oxide (BET surface area 94 m²/g). Simulated NH₄⁺ and PO₄³⁻ containing wastewater was prepared by adding various concentrations (600 ppm) of MAP (Fisher Scientific, Certified ACS) at room temperature with constant stirring at 350 rpm. Solutions ranging in concentrations from 100 to 2000 ppm MgO were added to the simulated wastewater and stirred for up to 240 min. The total volume of reactive solution was 500 mL. A volume of 1 mL of solution was sampled periodically and filtered through a 13 mm diameter PES filter (0.22 μ m pore size) to remove solid material and analyzed using ion chromatography. Concentrations of 100 ppm MgO and 600 ppm MAP used in this work correspond to a molar [Mg²⁺]: $[NH_4^+]:[PO_4^{3-}]$ ratio of 0.48:1:1, while 2000 ppm MgO and 600 ppm MAP correspond to a molar $[Mg^{2+}]:[NH_4^+]:[PO_4^{3-}]$ ratio of 9.51:1:1. $Mg^{2+}:NH_4^+:PO_4^{3-}$ ratios of 0.5–1.5:1:1 have previously been tested, and it was concluded that lower ratios lead to lesser N, P, and COD removal. 33,26,40,28 The concentration of 600 ppm MAP represents PO₄³⁻ and NH₄⁺ values found in municipal, animal, and industrial wastewater¹⁵ while maintaining a molar 1:1 ratio is needed for struvite formation. Therefore, a slight excess of Mg²⁺ was preferred

in the previous works to circumvent this issue and ensure efficient removal of N and P from the solution. $^{28,41}\,$

Solubility Index (SI) Calculations. Visual Minteq 3.1^{42} software was used to calculate saturation index values of the potential solid products at equilibrium. The pH in each case was set to initial experimental pH measured in each synthesis and was as follows: MgO (ppm), pH = 1000, 8.71; 500, 8.40; 300, 7.60; 100, 6.63). The ionic strength was not fixed but rather calculated from the ion balance. Concentrations of 100 ppm of $\mathrm{NH_4}^+$ and 500 ppm $\mathrm{PO_4}^{3-}$ were kept constant in all calculations while the Mg^{2+} ion concentration was set to that of the Mg from the initial MgO. Temperature of 25 °C was used to mimic experimental conditions.

 $\mathsf{PO_4}^{3-}$ **Adsorption Kinetics.** Pseudo-second-order ⁴³ kinetic models were used to analyze the obtained $\mathsf{PO_4}^{3-}$ adsorption data. In particular, the kinetic model parameters obtained by linear plot of t/q_t vs t for the pseudo-second-order model in eq 3 were used:

$$\frac{t}{q_{\rm t}} = \frac{1}{k_2 q_{\rm e}^2} + \frac{t}{q_{\rm e}} \tag{3}$$

where q_t (mg g⁻¹) and q_e (mg g⁻¹) are the amounts of PO₄³⁻ adsorbed at time t (min) and at equilibrium, respectively, while k_2 (g mg⁻¹ min⁻¹) is the rate constant of pseudo-second-order kinetic models.

■ RESULTS AND DISCUSSION

Kinetic Studies of Struvite Formation Using MgO. Ion chromatography was used to monitor the time dependent anion (PO_4^{3-}) and cation (NH_4^+) and Mg^{2+} concentration change taking place in the liquid phase of the reaction vessel

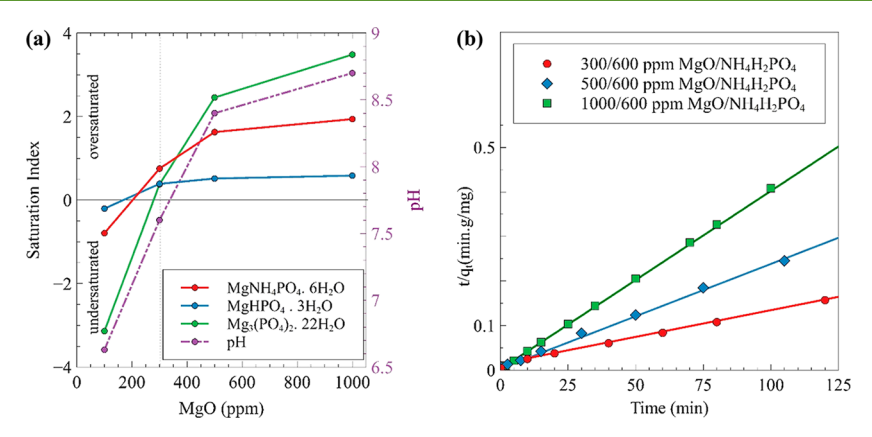


Figure 2. (a) Saturation Index calculations as a function of starting MgO concentration. (b) Kinetic modeling of experimental data using pseudo-second-order kinetics model for different starting concentrations of MgO.

during the formation of struvite product. Figure 1a shows the concentration profile of residual PO43- ions with three different initial MgO concentrations of 100, 300, and 1000 ppm which correspond to molar [Mg²⁺]:[NH₄⁺]:[PO₄³⁻] ratios of 0.48:1:1, 1.4:1:1, and 4.8:1:1, respectively. The concentration profiles of PO₄³⁻ anion show a steep decrease in the cases of 1000 and 300 ppm MgO, but no change is observed using 100 ppm MgO. The 1000 ppm MgO exhibited the fastest rate of PO₄³⁻ removal with PO₄³⁻ being almost completely removed after 50 min. In the case of 300 ppm MgO, the rate of PO₄³⁻ removal was slower and the final PO₄³⁻ concentration was ~40 ppm within 180 min approaching equilibrium. Concentration profiles of Mg²⁺ in solution as a function of reaction time in Figure 1b show that, for 1000 ppm MgO, the Mg²⁺ concentration decreased sharply for the first 10 min after which the rate of Mg²⁺ consumption slowed down. The final Mg^{2+} concentration of ~ 15 ppm was achieved within 80 min. For 300 ppm MgO, the rate of Mg²⁺ release followed by consumption was slower. Finally, for 100 ppm MgO, Mg²⁺ concentration increased to a steady state 45 ppm instead of decreasing, meaning that Mg²⁺ was produced rather than consumed. While the exact initial concentration is difficult to determine, an apparent initial hydrolysis reaction of MgO with water takes place within few minutes after the solid MgO introduction. The time resolved plot of NH₄⁺ shown in Figure 1c exhibits an interesting transient behavior in 1000 ppm MgO case. In particular, the rate of NH₄⁺ removal was very steep initially, but slowed with time. More importantly, the NH₄⁺ concentration in solution decreased sharply for 5 min increasing afterwards yielding the same equilibrium concentration as for the 100 ppm MgO experiment. Here, 300 ppm MgO in the equilibrium condition showed about 80% NH₄⁺ removal. Noteworthy, this equilibrium was achieved only after 100 min of the reaction time while the transient NH₄⁺ concentration decrease in the 1000 ppm case was much faster. Increase in initial MgO concentration agreed well with the increasing pH of the solution shown in Figure 1d. Here the initial 600 MAP solution pH was 5.4 and the first measurement with MgO added was taken 1-2 min after the addition. Results show that while pH increased in all three cases, 100 ppm MgO exhibited a gradual change from 6.6 to 7.0 pH over the total time of 250 min. On the other hand, 300 and 1000 ppm MgO showed much larger pH changes, with final pH values of 9.4 and 10.5, respectively. The former facilitated dissolution of MgO since no solid phase was formed via reaction with PO_4^{3-} .

To rationalize why only 300 ppm MgO ($[Mg^{2+}]$: $[NH_4^+]$: $[PO_4^{3-}] = 1.44:1:1)$ but no other MgO concentrations resulted in a stable, nontransient NH₄⁺ removal from aqueous solution, we performed equilibrium calculations using Visual MINTEQ version 3.1 software. 42 In particular, the effect of starting MgO concentration on the saturation index (SI) was analyzed using fundamental thermodynamic data listed in the literature. Solid product species considered were Mg₃(PO₄)₂· 22H₂O, MgHPO₄·3H₂O and struvite (MgNH₄PO₄·6H₂O) as a function of the initial Mg²⁺ concentration. Additionally, only initial (starting) experimental pH was considered and plotted in Figure 2a as it evolved during the MgO hydrolysis. Our analysis clearly shows that for MgO 300 ppm [Mg²⁺]:[NH₄⁺]: $[PO_4^{3-}]$ = 1.44:1:1 struvite exhibited the highest saturation index value. Lower concentrations, namely 100 ppm MgO, did not result in SI sufficient to obtain solid material, in agreement with Figure 1b where Mg²⁺ was shown to partition into solution. MgO concentrations higher than 300 ppm, namely, 500, 1000, 1500, and 2000 ppm, resulted in a solid phase with the highest saturation index of Mg₃(PO₄)₂·22H₂O. These results not only corroborate our time-resolved aqueous speciation, but also elucidate time and spatially resolved solid product analysis of the products (vide infra). Collectively, data shown in Figures 1 and 2a suggest that either a narrow MgO concentration regime needs to be obeyed to achieve maximum 80% removal of NH₄⁺ at the equilibrium or a fast kinetic regime can be utilized 5 min after the reaction onset to achieve \sim 70% removal of NH₄⁺.

To further evaluate the capacity of MgO to react with and remove both nutrient containing ions in a solid material form, kinetics of the PO_4^{3-} adsorption processes were analyzed. Removal of PO_4^{3-} was monitored as a function of time for three different starting concentrations of MgO (300, 500, and 1000 ppm) and fitted to a pseudo-second-order kinetics. The plot of t/q_t vs 1/t, as shown in Figure 2b, was used to extract q_e (mg g^{-1}), the amount of PO_4^{3-} adsorbed at equilibrium, and k_2 (g mg $^{-1}$ min $^{-1}$), the rate constant of pseudo-second-order adsorption reaction. These values are tabulated in Table 1.

The q_e values calculated using the t/q_e vs t plot for 300, 500, and 1000 ppm MgO were 833, 500, and 244 mg $\rm g^{-1}$, respectively, as shown in Table 1. These values show that as starting MgO concentration increased, the equilibrium concentration of $\rm PO_4^{~3^-}$ species decreased. In the literature, when the same model was applied to similar struvite growth kinetics using MgO-loaded diatomite, with a starting MgO concentration of 300 ppm, the q_e reported was significantly

Table 1. Calculated $q_{\rm e}$ (mg g⁻¹) and k_2 (g mg⁻¹ min⁻¹) Values for PO₄³⁻ Adsorption Using 300, 500, and 1000 ppm MgO

MgO concn (ppm)	$q_{\rm e}~({\rm mg~g^{-1}})$	$k_2 \; (\mathrm{g} \; \mathrm{mg}^{-1} \; \mathrm{min}^{-1})$	R^2
300	833	0.0001	0.99
500	500	0.00125	0.99
1000	244	0.08	1.00

lower with a value of 168 mg g⁻¹.³⁴ Moreover, the k_2 values calculated for 300, 500, and 1000 ppm MgO concentrations in our investigation were 0.0001, 0.00125, and 0.08 g mg⁻¹ min⁻¹, respectively, suggesting faster adsorption kinetics as MgO concentration increases. However, in the literature, at 300 ppm of MgO-diatomite adsorbent, an 8 times larger k_2 value of 0.0008 g mg⁻¹ min⁻¹ was reported.³⁴ This difference in k_2 values might stem from the fact that, in literature, MgO-diatomite, a highly porous, large surface area adsorbent material, was used instead of pure MgO used in this investigation. Lastly, at all concentrations of MgO tested in this study, the correlations based on the pseudo-second-order kinetic model showered almost perfect fits with $r^2 > 0.99$.

Solid Phase Product Bulk pXRD Analysis of 300 ppm MgO Reaction Products. To determine the identity of the solid product and the conversion rate of the reactants (MAP and MgO), pXRD analysis was performed. Simulated theoretical pXRD patterns of the potential solid products, namely, MgNH₄PO₄·6H₂O (PDF#15-0762), Mg₃PO₄·22H₂O (PDF 35-0186), and MgHPO₃·3H₂O (PDF 35-0780) were compared to the obtained experimental patterns. Solid products after 2 and 4 h were analyzed. pXRD patterns of both samples exhibited identical peaks that matched closely with the theoretical XRD pattern of MgNH₄PO₄·6H₂O (struvite) showing that insoluble MgO can be used to synthesize struvite. Importantly, no MgO peak at $2\theta = 42^{\circ}$ was observed, showing a complete conversion of the solid reactant. While confirming bulk identity of the solid product, however, data in Figure 3 did not provide additional insights on the fate of the above-stoichiometric Mg^{2+} that was present if all of the 300 ppm MgO reacted according to the molar ratio of $[Mg^{2+}]:[N\hat{H}_4^+]:[PO_4^{3-}] = 1.4:1:1$. Residual Mg^{2+} in solution at the equilibrium shown in Figure 1b varied little with the initial MgO concentration (only 15-18 ppm after 2 h for 300 and 1000 ppm, respectively), suggesting a potentially noncrystalline amorphous solid phase formed as a product that is not detectable with pXRD.

Effect of the Initial pH on the Liquid and Solid Product Speciation. To further understand the growth mechanism of struvite from insoluble MgO precursor in the kinetically controlled growth regime, the effect of the initial solution pH was studied while keeping the starting MgO concentration fixed at 1000 ppm. In particular, the initial pH of 8.5 was utilized by adjusting with NaOH to obtain data shown in Figure 4a and b while data shown in Figure 4c and d were obtained utilizing 0.1 M NaCO₃/NaHCO₃ buffer with pH of 9.2. These scenarios represent pH and buffering conditions typically needed to precipitate struvite at pH 7.5-9.0 in naturally buffered nutrient containing wastewater.²⁸ IC data in Figure 4a show the transient behavior of the initial NH₄+ consumption that switches to NH₄⁺ release after 5 min. A stark difference that is observed in Figure 4a is PO₄³⁻ consumption rate. When reaction took place with the initial pH of 8.5, PO₄³⁻ consumption slowed down significantly with the final concentration at 120 ppm after 125 min. No Mg²⁺ is released into solution. Time resolved solid product analysis using pXRD after 5, 60, and 120 min in Figure 4b shows that chiefly struvite is present after 5 min. However, fraction of unreacted MgO can also be detected. For samples corresponding to 60 and 120 min, pXRD pattern showed presence of Mg₃PO₄. 22H2O with virtually no struvite. Buffered experiments shown in Figure 4c and d still exhibited the transient change in NH₄⁺ concentration, with PO₄³⁻ consumption rate decreasing after 50 min at 20 ppm. Notably, Mg²⁺ concentration increased sharply until 55 min with the final equilibrium value of ~350 ppm. pXRD analysis of the solid products showed a mixture of struvite and Mg₃PO₄·22H₂O. No solid MgO phase was observed after 120 min synthesis. Based on IC analysis and XRD data of corresponding samples, it is seen that struvite species are produced initially when 1000 ppm MgO is used, irrespective of pH adjustment, which only alters the rate of this generation slightly. However, at longer reaction times, the major product of the synthesis is Mg₃PO₄·22H₂O. These results are also in line with our saturation index model predictions, shown in Figure 2.

Spatially Resolved Raman Spectroscopy of the Solid Reaction Products. Raman spectroscopy was used to analyze the compositional sample surface structure. It is different from routinely used pXRD analysis that is intrinsically a bulk

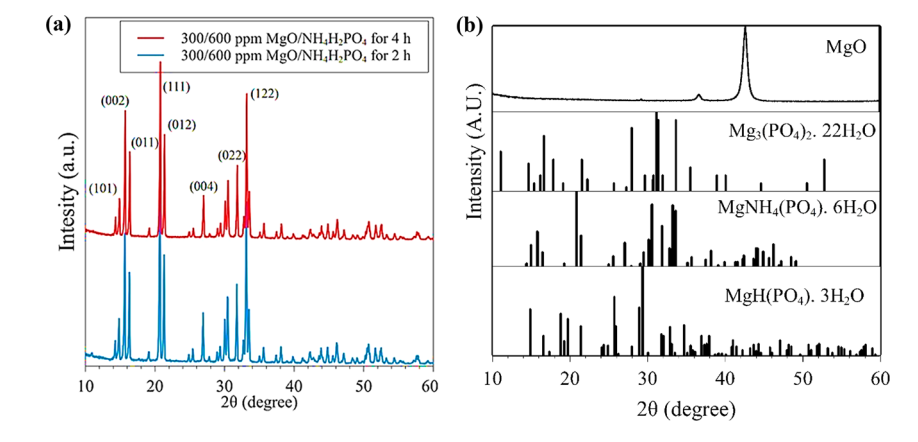


Figure 3. (a) pXRD patterns of solid products formed from 300 ppm MgO and 600 MAP. (b) Simulated patterns for MgO as well as the three main reaction products, $MgNH_4PO_4$ · $6H_2O$ (PDF#15-0762), $MgHPO_4$, Mg_3PO_4 · $22H_2O$ (PDF 35-0186), and $MgHPO_3$ · $3H_2O$ (PDF 35-0780) are also shown.

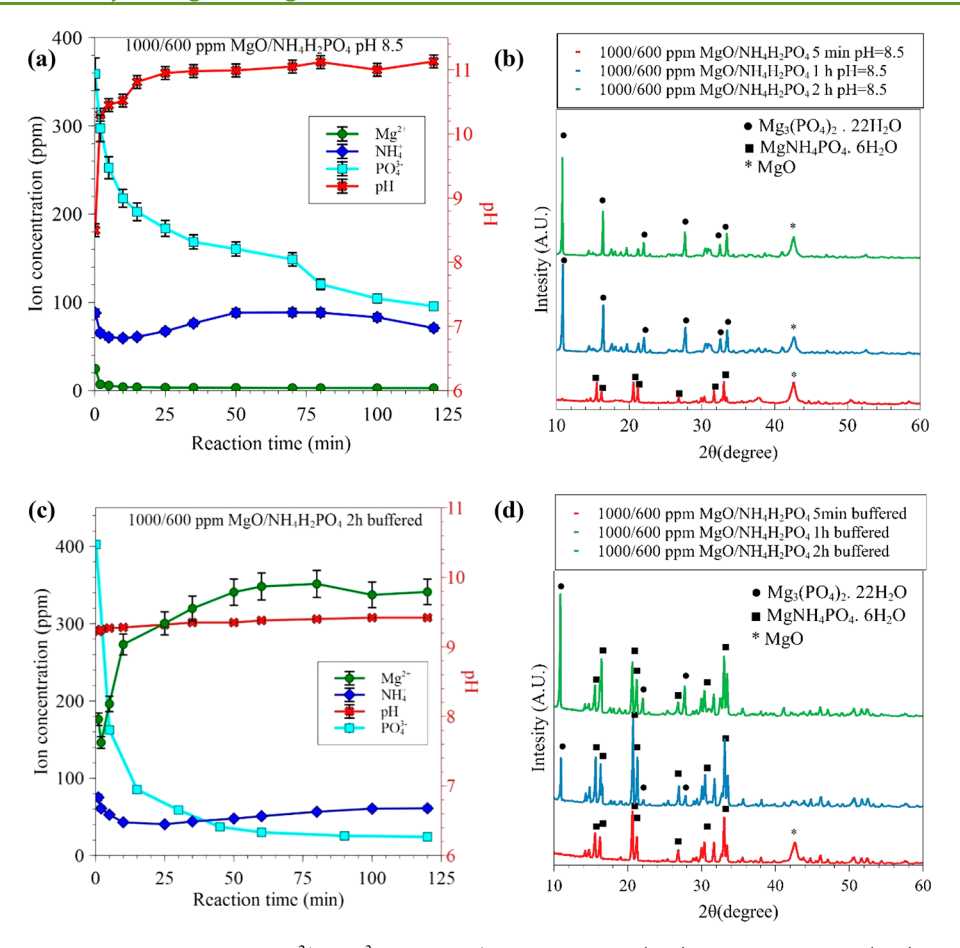


Figure 4. Time resolved concentration profiles of Mg^{2+} , $PO_4^{\ 3-}$, and $NH_4^{\ +}$ ion obtained at (a, b) initial pH 8.5 and (c, d) 0.1 M $NaCO_3/NaHCO_3$ buffered with pH of 9.2.

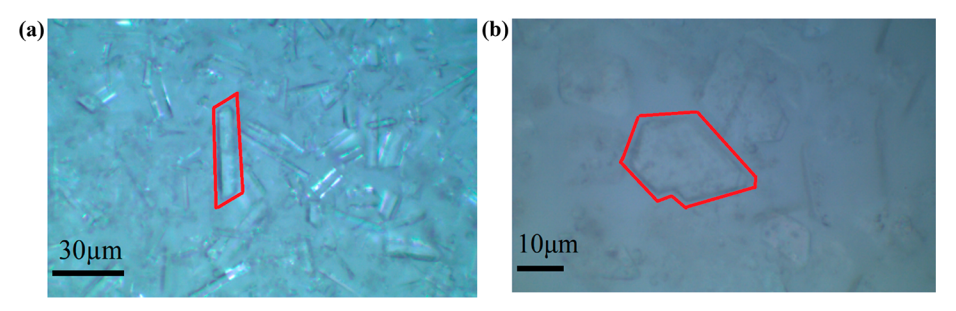


Figure 5. Optical images of solid reaction products obtained after: (a) 2 h reaction using 300/600 ppm $MgO/NH_4H_2PO_4$ and (b) 2 h reaction using 1000/600 ppm $MgO/NH_4H_2PO_4$.

measurement. Raman spectroscopy is especially suited for struvite analysis since it is sensitive to symmetric vibrations of the relevant ions, including PO_4^{3-} or $CO_3^{2-.32}$ In the previous work it was shown that a struvite sample synthesized using aqueous NH_4^+ and PO_4^{3-} precursors and water-soluble $MgCl_2$ exhibited Raman bands at 101, 144, 189, 229, 297, 393, 440, 570, 700, 750, 950, 981, 1020, 1125, 1429, 1469, 1675, 2357, a broad band at 2800–3430, 3498, and 3603 cm^{-1,32} The bands from 101 through 570 cm⁻¹ were attributed to the skeletal vibrations of struvite. 32,44 A sharp, prominent band at ~950 cm⁻¹ and smaller bands at 981 and 1020 cm⁻¹ were attributed to the symmetric and asymmetric PO_4^{3-} stretches, respectively. Two prominent peaks in 1400–1700 cm⁻¹ region were assigned to the deformational vibrations of NH_4^+ tetrahedra. Lastly, a broad band corresponding to different

N–H and O–H (in $\rm H_2O$) stretches is clearly seen in the 2200–3600 cm⁻¹ region and this broadness arises out of extensive hydrogen bonding. Any surface OH groups not participating in the hydrogen bonding network will be observed as a narrow, sharp band at ~3650 cm⁻¹.

Optical images acquired of solid reaction products obtained in this work showed diversity of the crystallites with two prevalent crystal shapes, as shown in Figure 5. In particular, solid reaction products with high overall NH₄⁺ ion removal rate, such as in 300/600 ppm MgO/NH₄H₂PO₄ after 2 h, or high initial NH₄⁺ ion removal rate, such as in 1000/600 ppm MgO/NH₄H₂PO₄ after 5 min, exhibited elongated coffinlike habit originating due to the fast (1 0 1) and (-1 0 1) facet growth as shown in Figure 5a. Experiments that did not yield significant NH₄⁺ ion removal, such as 1000/600 ppm MgO/

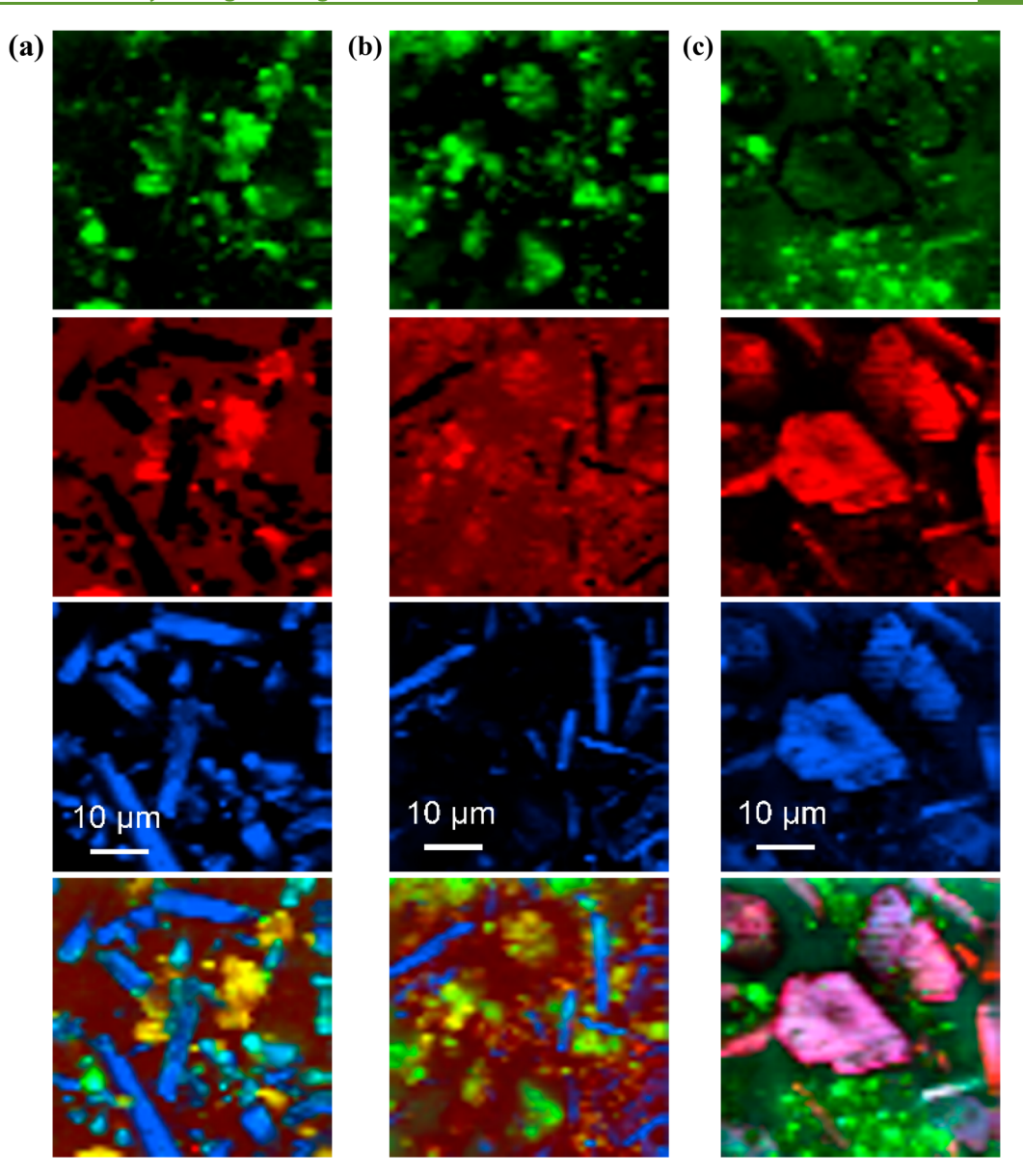


Figure 6. Large area Raman TCA maps of solid MgO reaction products and intermediates obtained from (a) 300/600 ppm MgO/NH₄H₂PO₄ after 2 h reaction, (b) 1000/600 ppm MgO/NH₄H₂PO₄ at initial pH 8.5 after 5 min reaction, and (c) 1000/600 ppm MgO/NH₄H₂PO₄ at initial pH 8.5 after 2 h reaction. The corresponding individual component Raman spectra are provided in Figure 7.

NH₄H₂PO₄ after 2 h, yielded significantly different platelet morphologies, as shown in Figure 5b. This morphology difference suggested two potential pathways during the crystallite growth. First, the kinetically controlled regime, potentially taking place under excess ([NH₄⁺]+[PO₄³⁻])/ $[Mg^{2+}]$ ratio, can be achieved since the initial $[Mg^{2+}]$ in solution is small and hence should be surface limited. Struvite formation using MgO has been shown to undergo series of surface transformations. In particular, hydration was observed with surface hydroxyl groups formed and measured spectroscopically.³² This was followed by pH decrease of the solution and a solid Mg(OH)₂ phase formation. CO₂ uptake typically results in pH decrease³³ and surface intermediate carbonate species cannot be ruled out. This would result in a crystal growth where the shapes of the crystal deviate from those favored thermodynamically via the formation of higher order (higher energy) planes. 47 This coincides with the elongated shape of the crystals shown in Figure 5a. However,

platelet morphology is uncommon during struvite growth 48,49 and crystal shape can be explained by formation of phosphates, such as $Mg_3PO_4\cdot 22H_2O$, consistent with pXRD data.

To further evaluate these possible products and, most importantly, reactive intermediates, we performed Raman spectroscopy in combination with TCA. The large area scans (LAS) shown in Figure 6 were obtained after spectral Raman maps were decomposed into three spectral components, color coded as blue, red, and green. Importantly, the blue component was unique, e.g., separate from the red one in (a) 300/600 ppm MgO/NH₄H₂PO₄ after 2 h reaction and (b) 1000/600 ppm MgO/NH₄H₂PO₄, initial pH 8.5 after 5 min reaction, while (c) 1000/600 ppm MgO/NH₄H₂PO₄ at initial pH 8.5 after 2 h reaction showed colocalization of the blue and the red component. The spectral footprints of all three components are shown in Figure 7.

In particular, the blue component corresponded to a typical struvite Raman spectrum with major bands at 285, 481, 565,

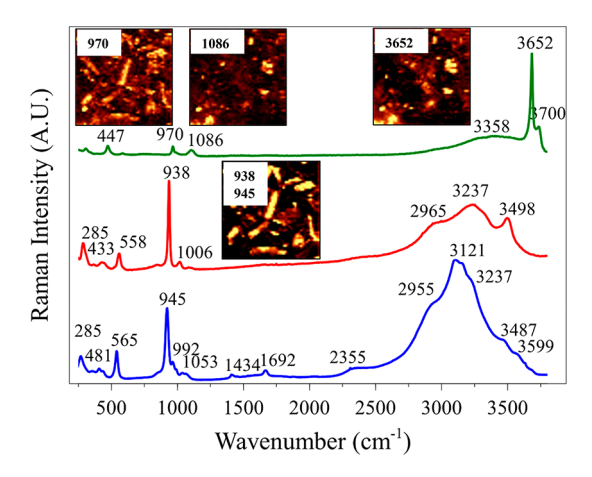


Figure 7. Principal spectral components obtained from TCA analysis from 300/600 ppm $MgO/NH_4H_2PO_4$ after 2 h, 1000/600 ppm $MgO/NH_4H_2PO_4$ at initial pH 8.5 after 5 min, and 1000/600 ppm $MgO/NH_4H_2PO_4$ at initial pH 8.5 after 2 h reaction.

945, 992, and 1053 cm⁻¹ and a structured, broad band at 2300-3600 cm⁻¹, with shoulders at 2355, 2955, 3121, 3237, 3487, and 3599 cm⁻¹. The 565 cm⁻¹ band corresponds to ν_4 bending of PO_4^{3-} , and the 945 cm⁻¹ band corresponds to ν_1 stretching of PO₄³⁻. The small 1663 cm⁻¹ band and the broad band with shoulders at 2955, 3121, 3237, and 3487 cm⁻¹ correspond to a mixture of vibrations of NH₄⁺ and H₂O molecules. The 3599 cm⁻¹ shoulder corresponds to the surface OH species on the Mg surface. The red component exhibits major bands at 285, 433, 558, 938, and 1006 cm⁻¹ and a structured, broad band at 2600-3600 cm⁻¹, with distinct shoulders at 2965, 3237, and 3498 cm⁻¹. The 938 and 1006 cm⁻¹ bands are due to the distorted PO₄³⁻ species, while the three shoulders at 2965, 3237, and 3498 can be assigned to complex water vibrational bands. Ammonia vibrational bands are absent and this spectral component is due to the magnesium phosphate. Lastly, the green component exhibited major bands at 447, 970, and 1086 cm⁻¹ and a structured, broad band in the 2700-3700 cm⁻¹ region with a shoulder at 3358 cm⁻¹ and two distinct sharp peaks at 3652 and 3700 cm⁻¹. The 970 band can be attributed to distorted vibrations of PO₄³⁻ species, while the two sharp bands at 3652 and 3700 cm⁻¹ likely arise from surface H₂O vibrations on surface $Mg(OH)_2$.

From Raman data presented in Figures 6 and 7, several reactive insights can be inferred. First, MgO surface indeed undergoes hydration³³ before adsorption of NH₄⁺ and PO₄³⁻ ions, as suggested by the unique green component obtained via TCA analysis. These intermediates possessed peaks unique to struvite (970 cm⁻¹), as well as some unrelated ones at 1086 cm⁻¹, which do not originate in struvite, as shown in the Figure 7 inset, but likely due to the carbonate. The latter is shifted to lower wavenumbers from that of pure MgCO₃ at 1125 cm^{-1 32} suggesting distortion of the CO_3^{2-} ion geometry. Similar peak was observed in dypingite, $Mg_5(CO_3)_4(OH)_2 \cdot 5H_2O$ at 1124 cm^{-1.50} Two sharp peaks at 3652 and 3700 cm⁻¹ can be attributed to the surface hydroxyl groups. They are much higher in frequency than structural OH vibrations found in other complex basic magnesium carbonate materials, such as hydromagnesite, $Mg_5(CO_3)_4(OH)_2 \cdot 4H_2O^{.51}$ The peak at 3651 cm⁻¹ was shown to be Raman active for pure $Mg(OH)_2$, ⁵² also present in Figure 7, green TCA component. This reactive intermediate is persistent even after 2 h of reaction, likely due

to the excess of ${\rm Mg^{2^+}}$ used for struvite precipitation as seen in Figure 6, and suggests an amorphous new intermediate of the reaction. Images shown in Figure 6 for 300/600 ppm MgO/NH₄H₂PO₄ after 2 h of reaction and 1000/600 ppm MgO/NH₄H₂PO₄ (initial pH 8.5) after 5 min of reaction time contained little of the red component. On the other hand, 1000/600 ppm MgO/NH₄H₂PO₄ (initial pH 8.5) after 2 h of reaction time contained mostly red and some of blue components, colocalized on platelet shaped particles. Both spectral components have peaks due to the symmetric PO₄³⁻ stretch at 945 and 938 cm⁻¹, respectively. The main difference was the absence of 1434 and 1692 cm⁻¹ peaks in the red component, suggesting absence of tetrahedral NH₄⁺ in the structure. This is consistent with the pXRD data where only the phosphate structural phase was present in this sample.

The spectral data presented so far reveal several important aspects of struvite formation using reactive low solubility transformations of MgO. A reactive intermediate detected by Raman as a complex magnesium hydroxyl carbonate that has a spectral footprint similar to dypingite - Mg₅(CO₃)₄(OH)₂· 4H₂O - is likely amorphous and hence nearly impossible to measure with pXRD. It can potentially contribute any missing mass needed to close the mass balance of struvite formation as it has few PO₄³⁻ groups in the structural unit. It further suggests that overall struvite formation kinetics can be improved by directly utilizing these abundant hydroxylated magnesium precursors, such as magnesite. Further, a potential route of first reacting MgO in water under controlled CO₂ atmosphere followed by reaction with NH₄⁺ and PO₄³⁻ ions can serve to enhance reaction kinetics of struvite formation via a two-step process to separate and accelerate the reactive steps. Finally, the latter approach can allow utilization of near stoichiometric [Mg²⁺]:[NH₄⁺]:[PO₄³⁻] avoiding use of excess magnesium reactant.

Economic Analysis of Struvite Synthesis Using MgO. While a variety of Mg sources have been utilized, reported MgO derived struvite costs are in general lower than those of MgCl₂ and MgSO₄. In particular, \$1050/ton of struvite was suggested using MgO while the costs to synthesize it from MgCl₂ and MgSO₄ were 6 and 3 times higher,³⁹ respectively, leading to somewhat unrealistic struvite prices. Depending on the locality and whether transportation was needed, MgSO₄ as raw material was about 10 times more expensive than rock minerals, such as magnesite (MgCO₃).⁵³ We performed economic analysis based on the different equilibrium and one kinetically driven struvite precipitation scenarios discussed above. Assumptions made in this economic evaluation were as follows:

- A typical farm employing manure flushing system will use anywhere from 240 to 620 gallons per day per animal.⁵⁴ On average, 430 gallons per day per animal is used for flushing manure. For this analysis, a farm with 1200 animals was assumed to generate 1.94 million L/ day nutrient containing wastewater;
- price of struvite was \$250 and \$350 per ton. The incomplete conversion of MgO shown in our spectral data set the upper price of the product to that of pure MgO (\$360 per ton);
- price of P was \$2/kg;⁵⁵
- price of N was \$1.2/kg;⁵⁵
- price of Mg was \$0.216/kg;
- price of MgO was \$360/ton;

all of the added MgO was transformed and left as Mg²⁺ or was converted into a solid struvite/phosphate. Our data above suggest as some of the unreacted reactive intermediate remains in the solid form even after equilibrium is achieved. Hence the calculations should be regarded as the upper (optimistic) limit approximation.

Economic calculations were performed on a mass balance basis, since raw material costs by far dominate any energy or capital costs. ⁵⁶ Unreacted NH₄⁺ and PO₄³⁻ leaving the process were considered to have an associated cost that would be incurred to further treat the wastewater. The data utilized for calculations are shown in Table 2 as scenarios 1–8.

Table 2. Economic Evaluation of Various Equilibrium and Kinetically Limited Struvite Formation Scenarios Using MgO as Magnesium Source

	final concn in solution after 120 min, mg/L (removal, %)			reaction conditions	
scenario	Mg ²⁺	NH ₄ ⁺	PO ₄ ³⁻	MgO/ NH ₄ H ₂ PO ₄ , ppm	Initial pH to final pH
1	43	90 (4)	452 (10)	100/600	5.4-6.8
2	12	21 (78)	37 (93)	300/600	5.4-9.3
3	12	88 (6)	7 (99)	500/600	5.4-10.1
4	16	92 (2)	5 (99)	1000/600	5.4-10.4
5	3	71 (24)	96 (81)	1000/600	8.5-11.2
6	340	60 (36)	24 (95)	1000/600 buffered ^a	9.2-9.4
7	151	47 (50)	84 (83)	500/600 buffered ^a	9.2-9.4
8	8	32 (66)	20 (96)	1000/600 after 5 min ^b	8.6-9.2

^aBuffering reagent costs were not accounted. ^bSolution composition for economic analysis was taken after 5 min of the reaction.

The economic evaluation based on the aforementioned assumptions resulted in two profitable scenarios with 300 ppm MgO added to precipitate struvite the most profitable as shown in Figure 8a. At all other MgO concentrations, the \$250/ton struvite cost resulted in a net loss. When a struvite

price of \$350/ton was considered, the kinetically controlled 1000 ppm regime was also profitable. Notably, \$350/ton was the upper limit to account for the incomplete conversion of MgO. Accordingly, mass balance also suggested product distribution of $[{\rm Mg^{2^+}}]:[{\rm NH_4}^+]:[{\rm PO_4}^{3^-}]=1:0.3:0.4$ while for the kinetically controlled case it was 1:0.08:0.1. The breakeven analysis of all scenarios in Table 2 was conducted to compute the corresponding price the struvite. The results of the analysis are shown in the Figure 8b. The data show that the breakeven curve passes through a minimum for the 300 ppm MgO scenario with a breakeven price of \$218/ton of struvite. All other scenarios have higher breakeven costs, and some such as scenario 1 (100 ppm MgO) yield high breakeven cost upward of \$5800/ton of struvite.

Sustainability Metrics of Substituting MgO as Magnesium Source for Struvite Precipitation. Magnesium chloride, (MgCl₂·xH₂O) mostly exists as MgCl₂·12H₂O in seawater (<1%).⁵⁷ MgCl₂ can have various degrees of hydration (x = 1, 2, 4, 6, 8, and 12) due to its hygroscopic nature. Accordingly, ~44,000 gallons of seawater need to be processed to produce a ton of hydrous MgCl₂ ⁵⁷ Moreover, the energy input required to produce MgCl2 via a typical industrial process involving concentrated brine feed is approximately 26,600 kWh/ton of Mg,³⁰ which is 19.6 tons of CO₂ equivalent produced per ton of Mg in the form of MgCl₂, assuming an average of 0.74 kg of CO₂ produced per kWh of electricity. On the other hand, the most employed MgO production routes are dead burning of magnesia (DBM), fusing of magnesia (FM), and caustic calcining of magnesia (CCM). MgO is mostly produced by thermal decomposition of natural minerals like dolomite (CaMg(CO₃)₂) and magnesite (MgCO₃).⁵⁹ The major energy input required for MgO production is for firing the furnaces and kilns with reported values between 2737 and 5313 kWh/ton of Mg produced in the form of MgO totaling to 2.0-3.9 tons of CO₂ equivalent, depending on various factors such as the type of calcination.⁵ An estimated 2000 kWh/ton of Mg produced in MgO form is also utilized for other processing steps such as crushing and filtering. These data are summarized in Figure 9. Collectively, these data show that MgO derived struvite, as opposed to MgCl₂ derived struvite, is more sustainable.

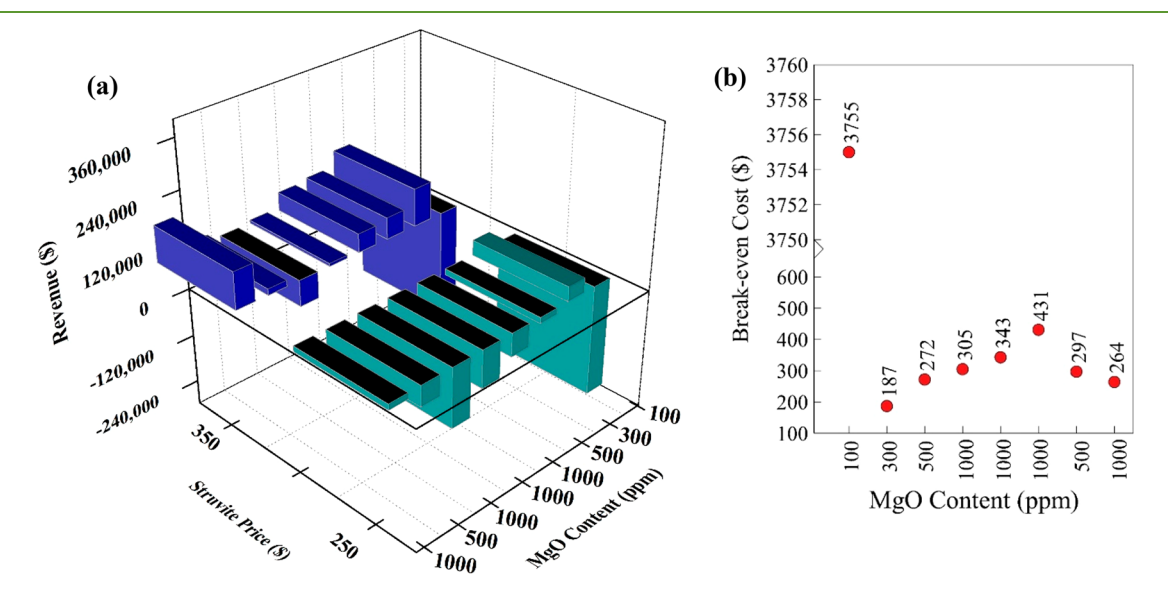
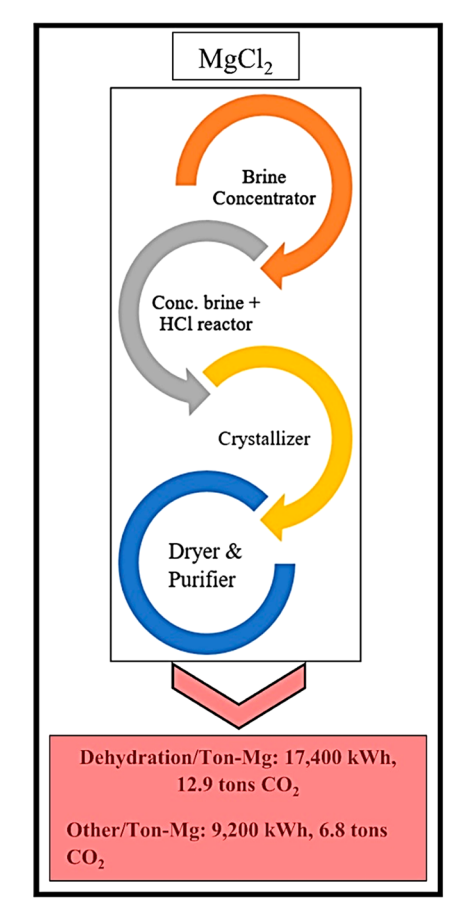


Figure 8. (a) Economic evaluation with revenues provided on an annual basis and (b) breakeven analysis of scenarios shown in Table 2.



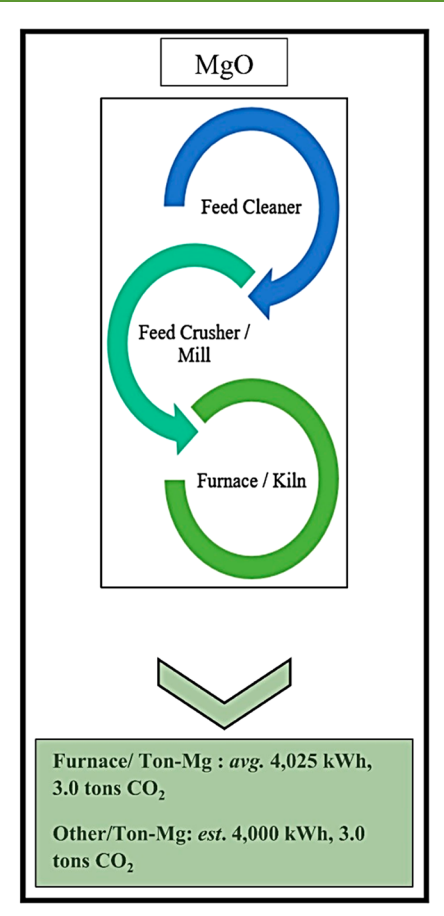


Figure 9. Schematic comparison of energy requirements and environmental impacts to produce struvite from wastewater using (left) MgCl₂ and (right) MgO.

CONCLUSIONS

In this investigation, we showed that water insoluble MgO precursor could be used to synthesize struvite (MgNH₄PO₄) instead of the conventional, water-soluble MgCl2 precursor. Literature analysis suggests that, due to the relative low solubility of MgO, increased Mg:P ratios are needed.³⁹ We show via time-resolved solid and liquid product speciation, kinetics, and modeling results that two MgO concentration regimes exist with the corresponding pseudo-second-order kinetics toward PO₄³⁻ removal that resulted in struvite formation: [Mg:NH₄⁺:PO₄³⁻] ratio of 1.4:1:1, with MgO concentration of 300 ppm, and [Mg:NH₄+:PO₄³⁻] ratio of 4.8:1:1, with MgO concentration of 1000 ppm, both with 600 ppm MAP. In the case of 300 ppm MgO, maximum removal of NH₄⁺ (80%) was achieved at equilibrium after ~2 h, while in the case of 1000 ppm MgO a fast kinetic regime can be observed 5 min after the reaction onset to achieve ~70% removal of NH₄⁺.

Spatially resolved Raman spectroscopic characterization of the solid reaction products after 300 ppm MgO in equilibrium and 1000 ppm MgO in kinetic regime reaction showed predominantly crystalline struvite with some intermediate species present. However, spatially resolved Raman spectra of product in the case of 1000 ppm MgO after 2 h in equilibrium showed a different product with less crystalline struvite and more amorphous intermediate species present. Spectra of the intermediate component, not detected with pXRD, were assigned to dypingite, $Mg_5(CO_3)_4(OH)_2\cdot 4H_2O$. This suggests that parallel hydration reaction takes place under ambient

conditions to form magnesium hydroxyl carbonates due to the excess of MgO. Additionally, it suggests that various carbonates of magnesium can potentially be utilized, with improved conversion toward struvite precipitation from aqueous MAP solutions, and will be utilized in the future work. Lastly, economic evaluation of struvite production using insoluble MgO precursor shows that the process would be economically viable only if the aforementioned concentration regimes are obeyed, namely, 300 ppm MgO at the equilibrium with 600 ppm MAP and 1000 ppm MgO with 600 ppm MAP under the kinetically controlled regime of 5 min reaction time. Sustainability analysis of struvite production from MgO clearly shows that employing MgO, instead of MgCl₂, for struvite production can significantly reduce energy requirements and the resulting carbon footprint by a factor of ~3.

AUTHOR INFORMATION

Corresponding Author

*E-mail: job314@lehigh.edu. Phone: 610-758-6836.

ORCID ®

Jonas Baltrusaitis: 0000-0001-5634-955X

Author Contributions

B.L. and Y.S. performed ion chromatography studies, D.B. and K.H. performed Raman and XRD studies, respectively, and Z.J. and D.K. performed theoretical modeling. Lastly, D.K. and J.B. performed experimental design, economic and sustainability calculations, and data analysis and wrote the manuscript.

Notes

The authors declare no competing financial interest.

ACKNOWLEDGMENTS

This material is based upon work supported by the National Science Foundation under Grant No. CHE 1710120.

REFERENCES

- (1) Foley, J. A.; Ramankutty, N.; Brauman, K. A.; Cassidy, E. S.; Gerber, J. S.; Johnston, M.; Mueller, N. D.; O'Connell, C.; Ray, D. K.; West, P. C.; et al. Solutions for a cultivated planet. *Nature* **2011**, 478, 337.
- (2) Foley, J. A.; Defries, R.; Asner, G. P.; Barford, C.; Bonan, G.; Carpenter, S. R.; Chapin, F. S.; Coe, M. T.; Daily, G. C.; Gibbs, H. K.; et al. Global Consequences of Land Use. *Science* **2005**, *309* (5734), 570–574.
- (3) Bouwman, L.; Goldewijk, K. K.; Van Der Hoek, K. W.; Beusen, A. H. W.; Van Vuuren, D. P.; Willems, J.; Rufino, M. C.; Stehfest, E. Exploring global changes in nitrogen and phosphorus cycles in agriculture induced by livestock production over the 1900–2050 period. *Proc. Natl. Acad. Sci. U. S. A.* 2013, 110 (52), 20882–20887.
- (4) Galloway, J. N.; Aber, J. D.; Erisman, J. W.; Seitzinger, S. P.; Howarth, R. W.; Cowling, E. B.; Cosby, B. J. The Nitrogen Cascade. *BioScience* **2003**, *53* (4), 341–356.
- (5) Galloway, J. N.; Cowling, E. B. Reactive Nitrogen and The World: 200 Years of Change. *Ambio* **2002**, *31* (2), 64–71.
- (6) Hicks, G. C.; Stinson, J. M. Pilot-Plant Production of Urea-Ammonium Sulfate. *Ind. Eng. Chem. Process Des. Dev.* **1975**, 14 (3), 269–276.
- (7) Luo, Y.; Li, H.; Huang, Y. R.; Zhao, T. L.; Yao, Q. Z.; Fu, S. Q.; Zhou, G. T. Bacterial mineralization of struvite using MgO as magnesium source and its potential for nutrient recovery. *Chem. Eng. J.* 2018, 351 (June), 195–202.
- (8) Cordell, D.; Rosemarin, A.; Schröder, J. J.; Smit, A. L. Towards global phosphorus security: a systems framework for phosphorus recovery and reuse options. *Chemosphere* **2011**, *84* (6), 747–758.
- (9) Lu, Y.; Academy, C. Phosphorus recovery: a need for an integrated approach Phosphorus recovery: a need for an integrated approach. *Ecosyst. Health Sustain.* **2018**, 4 (April), 48–57.
- (10) Baltrusaitis, J. Sustainable Ammonia Production. ACS Sustainable Chem. Eng. 2017, 5 (11), 9527–9527.
- (11) Patil, B. S.; Wang, Q.; Hessel, V.; Lang, J. Plasma N2-fixation: 1900–2014. Catal. Today 2015, 256 (Part 1), 49–66.
- (12) Gilbert, N. The disappearing nutrient. *Nature* **2009**, *461* (7265), 716–718.
- (13) Elser, J. J. Phosphorus: A limiting nutrient for humanity? *Curr. Opin. Biotechnol.* **2012**, 23 (6), 833–838.
- (14) Heilmann, S. M.; Molde, J. S.; Timler, J. G.; Wood, B. M.; Mikula, A. L.; Vozhdayev, G. V.; Colosky, E. C.; Spokas, K. A.; Valentas, K. J. Phosphorus reclamation through hydrothermal carbonization of animal manures. *Environ. Sci. Technol.* **2014**, 48 (17), 10323–10329.
- (15) Cai, T.; Park, S. Y.; Li, Y. Nutrient recovery from wastewater streams by microalgae: Status and prospects. *Renewable Sustainable Energy Rev.* **2013**, *19*, 360–369.
- (16) Booker, N. A.; Priestley, A. J.; Fraser, I. H. Struvite Formation in Wastewater Treatment Plants: Opportunities for Nutrient Recovery. *Environ. Technol.* **1999**, *20* (7), 777–782.
- (17) Bhuiyan, M. I. H.; Mavinic, D. S.; Beckie, R. D. A Solubility and Thermodynamic Study of. *Environ. Technol.* **2007**, 28 (9), 1015–1026.
- (18) Mehta, C. M.; Khunjar, W. O.; Nguyen, V.; Tait, S.; Batstone, D. J. Technologies to Recover Nutrients from Waste Streams: A Critical Review. *Crit. Rev. Environ. Sci. Technol.* **2015**, 45 (4), 385–427.
- (19) Talboys, P. J.; Heppell, J.; Roose, T.; Healey, J. R.; Jones, D. L.; Withers, P. J. A. Struvite: a slow-release fertiliser for sustainable phosphorus management? *Plant Soil* **2016**, 401 (1), 109–123.

- (20) Bouropoulos, N. C.; Koutsoukos, P. G. Spontaneous precipitation of struvite from aqueous solutions. *J. Cryst. Growth* **2000**, 213 (3-4), 381-388.
- (21) Ohlinger, K. N.; Young, T. M.; Schroeder, E. D. Predicting struvite formation in digestion. *Water Res.* **1998**, 32 (12), 3607–3614.
- (22) Ronteltap, M.; Maurer, M.; Hausherr, R.; Gujer, W. Struvite precipitation from urine Influencing factors on particle size. *Water Res.* **2010**, *44* (6), 2038–2046.
- (23) Stratful, I.; Scrimshaw, M. D.; Lester, J. N. Conditions influencing the precipitation of magnesium ammonium phosphate. *Water Res.* **2001**, *35* (17), 4191–4199.
- (24) Britton, A.; Koch, F. A.; Mavinic, D. S.; Adnan, A.; Oldham, W. K.; Udala, B. Pilot-scale struvite recovery from anaerobic digester supernatant at an enhanced biological phosphorus removal wastewater treatment plant. *J. Environ. Eng. Sci.* **2005**, *4* (4), 265–277.
- (25) Hövelmann, J.; Putnis, C. V. In Situ Nanoscale Imaging of Struvite Formation during the Dissolution of Natural Brucite: Implications for Phosphorus Recovery from Wastewaters. *Environ. Sci. Technol.* **2016**, *50* (23), 13032–13041.
- (26) Ishii, S. K. L.; Boyer, T. H. Life cycle comparison of centralized wastewater treatment and urine source separation with struvite precipitation: Focus on urine nutrient management. *Water Res.* **2015**, 79, 88–103.
- (27) Senbayram, M.; Gransee, A.; Wahle, V.; Thiel, H. Role of magnesium fertilisers in agriculture: plant—soil continuum. *Crop Pasture Sci.* **2015**, *66* (12), 1219.
- (28) Rahman, M. M.; Salleh, M. A. M.; Rashid, U.; Ahsan, A.; Hossain, M. M.; Ra, C. S. Production of slow release crystal fertilizer from wastewaters through struvite crystallization A review. *Arabian J. Chem.* **2014**, *7* (1), 139–155.
- (29) Ramakrishnan, S.; Koltun, P. A Comparison of the Greenhouse Impacts of Magnesium Produced By Electrolytic and Pidgeon Processes. In *Essential Readings in Magnesium Technology*; Mathaudhu, S. N., Luo, A. A., Neelameggham, N. R., Nyberg, E. A., Sillekens, W. H., Eds.; Springer International Publishing: Cham, 2016; pp 169–174.
- (30) Liu, J.; Bearden, M. D.; Fernandez, C. A.; Fifield, L. S.; Nune, S. K.; Motkuri, R. K.; Koech, P. K.; McGrail, B. P. Techno-Economic Analysis of Magnesium Extraction from Seawater via a Catalyzed Organo-Metathetical Process. *JOM* 2018, 70 (3), 431–435.
- (31) USGS. Mineral Commodity Summaries; U.S. Geological Survey, 2017.
- (32) Kirinovic, E.; Leichtfuss, A. R.; Navizaga, C.; Zhang, H.; Christus, J. D. S.; Baltrusaitis, J. Spectroscopic and microscopic identification of the reaction products and intermediates during the struvite (MgNH4PO4·6H2O) formation from magnesium oxide (MgO) and magnesium carbonate (MgCO3) microparticles. ACS Sustainable Chem. Eng. 2017, 5 (2), 1567–1577.
- (33) Stolzenburg, P.; Capdevielle, A.; Teychené, S.; Biscans, B. Struvite precipitation with MgO as a precursor: Application to wastewater treatment. *Chem. Eng. Sci.* **2015**, *133*, 9–15.
- (34) Xia, P.; Wang, X. X. X.; Wang, X. X. X.; Song, J.; Wang, H.; Zhang, J.; Zhao, J. Struvite crystallization combined adsorption of phosphate and ammonium from aqueous solutions by mesoporous MgO-loaded diatomite. *Colloids Surf., A* **2016**, *506*, 220–227.
- (35) Capdevielle, A.; Sýkorová, E.; Biscans, B.; Béline, F.; Daumer, M. L. Optimization of struvite precipitation in synthetic biologically treated swine wastewater-Determination of the optimal process parameters. *J. Hazard. Mater.* **2013**, 244–245, 357–369.
- (36) Romero-Güiza, M. S.; Astals, S.; Mata-Alvarez, J.; Chimenos, J. M. Feasibility of coupling anaerobic digestion and struvite precipitation in the same reactor: Evaluation of different magnesium sources. *Chem. Eng. J.* **2015**, 270, 542–548.
- (37) Chimenos, J. M.; Fernández, A. I.; Villalba, G.; Segarra, M.; Urruticoechea, A.; Artaza, B.; Espiell, F. Removal of ammonium and phosphates from wastewater resulting from the process of cochineal extraction using MgO-containing by-product. *Water Res.* **2003**, *37* (7), 1601–1607.

- (38) Kim, J. H.; An, B. m.; Lim, D. H.; Park, J. Y. Electricity production and phosphorous recovery as struvite from synthetic wastewater using magnesium-air fuel cell electrocoagulation. *Water Res.* **2018**, *132*, 200–210.
- (39) Hug, A.; Udert, K. M. Struvite precipitation from urine with electrochemical magnesium dosage. *Water Res.* **2013**, 47 (1), 289–299.
- (40) Yetilmezsoy, K.; Sapci-Zengin, Z. Recovery of ammonium nitrogen from the effluent of UASB treating poultry manure wastewater by MAP precipitation as a slow release fertilizer. *J. Hazard. Mater.* **2009**, *166* (1), 260–269.
- (41) Zhang, T.; Ding, L.; Ren, H. Pretreatment of ammonium removal from landfill leachate by chemical precipitation. *J. Hazard. Mater.* **2009**, *166* (2–3), 911–915.
- (42) Gustafsson, J. P. Visual MINTEQ 3.0 user guide; 2011, pp 1-73.
- (43) Ho, Y. S.; McKay, G. Pseudo-second order model for sorption processes. *Process Biochem.* **1999**, 34 (5), 451–465.
- (44) Frost, R. L.; Weier, M. L.; Martens, W. N.; Henry, D. A.; Mills, S. J. Raman spectroscopy of newberyite, hannayite and struvite. *Spectrochim. Acta, Part A* **2005**, *62* (1–3), 181–188.
- (45) Prywer, J.; Kasprowicz, D.; Runka, T. Temperature-dependent μ -Raman investigation of struvite crystals. *Spectrochim. Acta, Part A* **2016**, 158, 18–23.
- (46) Prywer, J.; Torzewska, A.; Plociński, T. Unique surface and internal structure of struvite crystals formed by Proteus mirabilis. *Urol. Res.* **2012**, *40* (6), 699–707.
- (47) Xia, Y.; Xiong, Y.; Lim, B.; Skrabalak, S. E. Shape-controlled synthesis of metal nanocrystals: Simple chemistry meets complex physics? *Angew. Chem., Int. Ed.* **2009**, 48 (1), 60–103.
- (48) Manzoor, M. A. P.; Singh, B.; Agrawal, A. K.; Arun, A. B.; Mujeeburahiman, M.; Rekha, P. D. Morphological and microtomographic study on evolution of struvite in synthetic urine infected with bacteria and investigation of its pathological biomineralization. *PLoS One* **2018**, *13* (8), e0202306.
- (49) Le Corre, K. S.; Valsami-Jones, E.; Hobbs, P.; Parsons, S. A. Impact of calcium on struvite crystal size, shape and purity. *J. Cryst. Growth* **2005**, 283 (3–4), 514–522.
- (50) Frost, R. L.; Bahfenne, S.; Graham, J. Raman spectroscopic study of the magnesium-carbonate minerals artinite and dypingite. *J. Raman Spectrosc.* **2009**, 40 (8), 855–860.
- (51) Frost, R. L. Raman spectroscopic study of the magnesium carbonate mineral hydromagnesite (Mg 5[(CO 3) 4(OH) 2]· 4H 2O). *J. Raman Spectrosc.* **2011**, 42 (8), 1690–1694.
- (52) Krishnamurti, D. The Raman and IR Spectra of Some Solid Hydroxides; 1959; pp 247–253.
- (53) Etter, B.; Tilley, E.; Khadka, R.; Udert, K. M. Low-cost struvite production using source-separated urine in Nepal. *Water Res.* **2011**, 45 (2), 852–862.
- (54) Harner, J. P.; Murphy, J. P. Flushing manure systems for dairy facilities. *Kansas Agric. Exp. Stn. Res. Reports* **1997**, 0 (2), 19–23.
- (55) Egle, L.; Rechberger, H.; Krampe, J.; Zessner, M. Phosphorus recovery from municipal wastewater: An integrated comparative technological, environmental and economic assessment of P recovery technologies. *Sci. Total Environ.* **2016**, *571*, 522–542.
- (56) Turton, R. et al. Analysis, Synthesis, and Design of Chemical Processes, 4th ed.; Prentice Hall, 2012.
- (57) Al Mutaz, I. S.; Wagialia, K. M. Production of magnesiumfrom desalination brines. *Resour. Conserv. Recycl.* **1990**, *3*, 231–239.
- (58) https://www.epa.gov/energy/greenhouse-gases-equivalencies-calculator-calculations-and-references, EPA.gov, 2018.
- (59) European Commission. Reference Document on Best Available Techniques in the Cement, Lime and Magnesium Oxide Manufacturing Industries. *Eur. Comm.* 2010, No. May, 459.